

Monte Carlo Simulations of Biaxial Molecules Near Hard Wall

Received: 04.10.2021 & Accepted: 15.11.2021

A. KAPANOWSKI* AND S. DAWIDOWICZ

*Faculty of Physics, Astronomy and Applied Computer Science, Jagiellonian University,
Łojasiewicza 11, 30-348 Kraków, Poland*

Doi: [10.12693/APhysPolA.140.365](https://doi.org/10.12693/APhysPolA.140.365)

*e-mail: andrzej.kapanowski@uj.edu.pl

A system of optimal biaxial molecules placed at the sites of a cubic lattice is studied in an extended Lebwohl–Lasher model. Molecules interact only with their nearest neighbors through the pair potential that depends on the molecule orientations. It is known that in a homogeneous system there is a direct second-order transition from the isotropic to the biaxial nematic phase, however the properties of confined systems are less known. In the present paper, the lattice has periodic boundary conditions in the X and Y directions and has two walls with planar anchoring, perpendicular to the Z direction. We have investigated the model using Monte Carlo simulations on $N_x \times N_y \times N_z$ lattices, for $N_x = N_y = 10, 16$, N_z from 3 to 19, with and without mirror symmetry. This study is complementary to the statistical description of hard spheroplatelets near a hard wall (*Phys. Rev. E* **89**, 062503 (2014)). The temperature dependence of the order-parameter profiles between walls is calculated for many cases of wall separations. For large wall separations, there are surface layers with biaxial ordering on both walls (≈ 4 – 5 lattice constants wide) and, beyond the surface layers, the order parameters have values as in a homogeneous system. For small wall separations, the isotropic–biaxial transition is shifted and the surface layers are thinner. Above the isotropic–biaxial transition the preferable orientations in both surface layers can be different. It is interesting that planar anchoring for biaxial molecules leads to uniaxial interactions on the wall. As a result, we get the planar Lebwohl–Lasher model with additional (biaxial) interactions with neighbors from the second layer, where the Kosterlitz–Thouless transition is present on the wall.

topics: liquid crystals, biaxial nematics, Monte Carlo simulations

1. Introduction

Biaxial nematic phases are characterized by an orientational order along three perpendicular directions ($\mathbf{L}, \mathbf{M}, \mathbf{N}$) and by the existence of three distinct optical axes. Such phases were first predicted by Freiser in 1970 [1]. Later, biaxial phases have been studied by mean field theory [2–4], counting methods (a generalization of Flory’s lattice model) [5, 6], bifurcation analysis [7], and other methods including computer simulations [8–10]. Motivation for these studies ranges from purely academic interest to the potential usage of biaxial nematics in displays with improved response times and better viewing characteristics [11, 12]. It was found that switching of the secondary axis is up to an order of magnitude faster than that of the principal axis.

Straley obtained a phase diagram for a system of biaxial molecules using mean field theory [2]. He showed that four order parameters are necessary to describe ordered phases with biaxial molecules.

The same was confirmed by Mulder who also derived the analytical formula for the excluded volume for a pair of spheroplatelets which are biaxial objects [13].

The first theories predict that a system of biaxial molecules can exhibit four phases, depending on the molecular biaxiality, i.e., positive uniaxial phase (N_{U+} , with prolate molecules), negative uniaxial phase (N_{U-} , with oblate molecules), biaxial phase (N_B), and isotropic phase (I). The nematic–isotropic phase transition is weakly first order and becomes continuous at the point of maximum molecular biaxiality. At this point there is a direct transition from the biaxial to the isotropic phase.

Later theories have showed that the phase transitions to the biaxial phase can be either first or second order with the possibility of several critical points and reentrant biaxial nematic phases [14]. In some phase diagrams three different biaxial phases were identified, where two additional biaxial phases were connected with mixtures of rodlike and plate-like molecules [15].

2. Previous computer studies

2.1. Lattice models

The Lebwohl–Lasher (LL) model is a lattice version of the Maier–Saupe model of anisotropic liquids with uniaxial molecules [16, 17]. A weak first-order nematic–isotropic phase transition was found in the three-dimensional model at $T^* = 1.1232(1)$ for lattice sizes up to $28 \times 28 \times 28$ [18]. Pretransitional fluctuations of the LL model were studied by Greff and Lee [19]. A large lattice of $120 \times 120 \times 120$ was studied on a parallel supercomputer and the temperature dependence of energy, order parameter and heat capacity was obtained with greater accuracy [20]. The effect of an external field on a nematic system was also investigated and a change in the character of the transition from the first to the second order with the disappearance of the transition at a critical point was observed.

A biaxial version of the LL model was studied by Biscarini et al. [21]. They determined the phase diagram of the lattice model for varying biaxiality. The full set of four second rank order parameters was calculated for the first time and the differences from mean field theory were discussed.

2.2. Molecules at interface

The properties of the nematic–isotropic phase transition in thin nematic films were studied for the first time by Sheng [22]. He used the Landau–de Gennes theory to show the existence of a critical film thickness below which the transition from the nematic phase to the isotropic phase becomes continuous. Later, this framework was used to describe a boundary-layer phase transition that occurs at temperatures higher than the bulk-transition temperature [23].

A thin cell with hard spherocylinders was studied by Mao et al. [24]. Spherocylinders are composed of cylinders of a length L , a diameter D , and hemispherical end caps. Grand canonical Monte Carlo simulations (MC) were used to investigate the effect of finite aspect ratio L/D in density profiles and in order parameters ($L/D = 10, 20$). The wall effect penetrated the bulk to a distance of order L . No biaxial order was present if the phase was isotropic in bulk in the simulated system. In the next paper by Mao et al. [25] the depletion force was studied in the confined geometry of two parallel plates.

In 2000, van Roij et al. [26, 27] investigated the phase behavior of hard-rod fluid near a single wall and confined in a slit pore. A wall-induced surface transition was observed from uniaxial to biaxial symmetry, as well as complete orientational wetting of the wall-isotropic fluid interface by the nematic film. Theoretical analysis was done by employing Zwanzig’s rod model where the molecules are restricted to orientations which are parallel to one of the Cartesian coordinate axes. The results were confirmed by Monte Carlo simulations of a fluid of hard spherocylinders with $L/D = 15$ [28].

Liquid crystals confined between parallel walls were studied by Allen [29]. Numerical simulations were compared with the theoretical predictions of Onsager’s density functional theory. Several different anchoring conditions on the wall-nematic interface were investigated. In all cases, the principal effect of increasing the average density is to increase the surface film thickness.

A density functional treatment of a hard Gaussian overlap fluid confined between two parallel hard walls was presented by Chrzanowska et al. [30]. For uniaxial particles of elongation 5, the density and order parameter profiles were obtained in the Onsager approximation. The surface layers of thickness about half of the particle length were present with uniaxial and biaxial order for the isotropic and uniaxial bulk phase, respectively.

The effect of the incomplete interaction on the nematic–isotropic transition at the nematic-wall interface was studied by Batalioto et al. [31]. They used an extended Maier–Saupe approach with additional interactions with the wall. In this framework, the existence of a boundary layer was demonstrated, in which the order parameter can be greater or smaller than that in the bulk, depending on the relation between the strength of the surface and nematic potentials.

The equilibrium phase behavior of a confined rigid-rod system was studied by Green et al. [32]. The distribution functions for stable and unstable equilibrium states were computed as a function of the system density and the width of the system. The surprising conclusion was that the introduction of walls perturbs the stability limits for any system width which means that walls always impact the interior of systems.

Aliabadi et al. [33] examined the ordering properties of *rectangular* hard rods on a single planar wall and between two parallel hard walls using the second virial density functional theory in the Zwanzig approximation [33]. The most interesting finding for the slit pore is the first-order transition from the surface ordered isotropic to the capillary nematic phase. This transition weakens with decreasing pore width and terminates in a critical point.

A system of hard spheroplatelets near a hard wall was studied in the low-density Onsager approximation by Kapanowski and Abram [34]. The spheroplatelets had optimal shape between rods and plates, and the direct transition from the isotropic to the biaxial nematic phase was present in the bulk. For the one-particle distribution function $\rho(z, R)$, a simple approximation was used and as a result, outside the surface layer the order parameters were equal to their bulk values. The width of the surface layer was equal to the half of the molecule diagonal length. Biaxiality close to the wall appeared only if the phase was biaxial in the bulk. For the case of the isotropic phase in the bulk, the phase near the wall was uniaxial (oblate).

Our aim in the present paper is to get more realistic order parameter profiles between two walls and check the width of the interfacial region for the system of biaxial molecules with a direct transition from the isotropic to the biaxial nematic phase. This paper is organized as follows. The lattice model of biaxial molecules is described in Sect. 3. In Sect. 4, we present the results of Monte Carlo simulations of the homogeneous and confined systems and Sect. 5 contains the summary.

3. System

We have considered a system of optimal biaxial molecules placed at sites of the cubic lattice $N_x \times N_y \times N_z$. The optimal hard biaxial molecules have the shape between the rods and the plates, and the direct transition from the isotropic to the biaxial nematic phase is present in the bulk. In our model, the molecule shape can be inferred indirectly from the interactions but the key feature is the direct $I-N_B$ transition. The orientation of a rigid molecule can be determined by several methods, i.e., by the three Euler angles $R = (\phi, \theta, \psi)$; by the three orthonormal vectors $(\mathbf{l}, \mathbf{m}, \mathbf{n})$, by the orthogonal rotation matrix; and by the unit quaternion [35]. We are using quaternions in simulations because they are compact, stable numerically, and we do not have to use trigonometric functions which are computationally expensive. Our calculations are based on the second rank pair potential [3, 21], i.e.,

$$U(R_{ij}) = -\epsilon_{ij} \left[F_{00}^{(2)}(R_{ij}) + \lambda F_{02}^{(2)}(R_{ij}) + \lambda F_{20}^{(2)}(R_{ij}) + \lambda^2 F_{22}^{(2)}(R_{ij}) \right], \quad (1)$$

where R_{ij} is the relative orientation of the molecule pair, ϵ_{ij} is equal to a positive constant ϵ for the nearest neighbors, and zero otherwise. The biaxiality parameter λ accounts for the deviation from the cylindrical molecular symmetry. For $\lambda = 0$, the Lebwohl-Lasher model is recovered. The value $\lambda = 1/\sqrt{3}$ marks the boundary between a system of prolate ($\lambda < 1/\sqrt{3}$) and oblate molecules ($\lambda > 1/\sqrt{3}$). In our study, we focus on the most biaxial molecules so $\lambda = 1/\sqrt{3}$. Note that $\lambda = \sqrt{2}\lambda'$, where λ' was used in [21]. The difference comes from different definitions of symmetry-adapted functions. The functions $F_{\mu\nu}^{(j)}$ are defined in [36] and they are related to Wigner functions $D_{\mu\nu}^{(j)}$. The most important functions are

$$F_{00}^{(2)}(R) = P_2(n_z), \quad (2)$$

$$F_{02}^{(2)}(R) = \frac{\sqrt{3}}{3} \left[P_2(l_z) - P_2(m_z) \right], \quad (3)$$

$$F_{20}^{(2)}(R) = \frac{\sqrt{3}}{3} \left[P_2(n_x) - P_2(n_y) \right], \quad (4)$$

$$F_{22}^{(2)}(R) = \frac{1}{3} \left[P_2(l_x) + P_2(m_y) - P_2(m_x) - P_2(l_y) \right], \quad (5)$$

where $P_2(x)$ is the second Legendre polynomial. For the completely ordered system with all molecule orientations parallel to the walls, we get $U = -3N\epsilon(1 + \lambda^2)$, where $N = N_x N_y N_z$ is the number of molecules (lattice sites).

We have performed Monte Carlo simulations with the following three different boundary conditions.

1. Periodic boundary conditions in the three directions are for the homogeneous system.
2. Periodic boundary conditions in the two directions X, Y , and the two walls at $z = 0$ and $z = (N_z - 1)a$ with planar anchoring are for the confined systems, and a is the lattice constant. The distance between the walls is $L_z = (N_z - 1)a$. In fact, we also get a periodic condition here in the Z direction, because we use the constant term for the missing neighbor on both walls.
3. Periodic boundary conditions in the two directions X, Y , the wall at $z = 0$ with planar anchoring, and mirror symmetry applied at $z = (N_z - 1)a$. This corresponds to $L_z = 2(N_z - 1)a$, but less computer resources are needed for simulations.

It appeared that in the case 3 we cannot update the system energy in the same way as in the cases 1 and 2, namely, molecules at $z = (N_z - 1)a$ and $z = (N_z - 2)a$ have to be analyzed separately. That is why we focus on the cases 1 and 2. Planar anchoring on the walls is motivated by the fact that elongated molecules can be closer to the wall only if they are parallel to it. On the other hand, the isotropic-nematic interface favors planar anchoring [29].

Now, let us determine the order parameters and their temperature dependence. In computer simulations of homogeneous systems, three tensors are typically used [8, 21]

$$Q_{\alpha\beta}^{ll} = \frac{3}{2N} \sum_{i=1}^N \left(l_{\alpha}^i l_{\beta}^i - \frac{1}{3} \delta_{\alpha\beta} \right), \quad (6)$$

$$Q_{\alpha\beta}^{mm} = \frac{3}{2N} \sum_{i=1}^N \left(m_{\alpha}^i m_{\beta}^i - \frac{1}{3} \delta_{\alpha\beta} \right), \quad (7)$$

$$Q_{\alpha\beta}^{nn} = \frac{3}{2N} \sum_{i=1}^N \left(n_{\alpha}^i n_{\beta}^i - \frac{1}{3} \delta_{\alpha\beta} \right). \quad (8)$$

Through the tensors diagonalization one could determine the order parameters according to the procedure described in [21]. A nontrivial problem is to find a consistent way of assigning the three eigenvalues to the X, Y, Z axes. In our confined systems, all three tensors $Q_{\alpha\beta}^{ll}$, $Q_{\alpha\beta}^{mm}$, $Q_{\alpha\beta}^{nn}$ are calculated independently for all layers parallel to the walls. Then the Z axis is always perpendicular to the walls, and the X axis is parallel to the walls and corresponds to the maximum eigenvalue of the tensor $Q_{\alpha\beta}^{nn}$. Finally, the four order parameters $\langle F_{\mu\nu}^{(2)} \rangle$ are calculated

$$\langle F_{00}^{(2)} \rangle = Q_{zz}^{nn} = -Q_{zz}^{ll} - Q_{zz}^{mm}, \quad (9)$$

TABLE I

Order parameters (OP) for the completely ordered systems. Orientations used for the homogeneous and the confined systems are marked.

OP	$\mathbf{N} Z, \mathbf{L} X$ (homogeneous)	$\mathbf{N} Z, \mathbf{L} Y$	$\mathbf{N} X, \mathbf{L} Z$ (confined)	$\mathbf{N} X, \mathbf{L} Y$	$\mathbf{N} Y, \mathbf{L} Z$	$\mathbf{N} Y, \mathbf{L} X$
$\langle F_{00}^{(2)} \rangle$	1	1	-1/2	-1/2	-1/2	-1/2
$\langle F_{02}^{(2)} \rangle$	0	0	$\sqrt{3}/2$	$-\sqrt{3}/2$	$\sqrt{3}/2$	$-\sqrt{3}/2$
$\langle F_{20}^{(2)} \rangle$	0	0	$\sqrt{3}/2$	$\sqrt{3}/2$	$-\sqrt{3}/2$	$-\sqrt{3}/2$
$\langle F_{22}^{(2)} \rangle$	1	-1	1/2	-1/2	-1/2	1/2

$$\sqrt{3}\langle F_{02}^{(2)} \rangle = Q_{zz}^{ll} - Q_{zz}^{mm} = -Q_{xx}^{ll} - Q_{yy}^{ll} + Q_{xx}^{mm} + Q_{yy}^{mm}, \quad (10)$$

$$\sqrt{3}\langle F_{20}^{(2)} \rangle = Q_{xx}^{nn} - Q_{yy}^{nn} = -Q_{xx}^{ll} - Q_{xx}^{mm} + Q_{yy}^{ll} + Q_{yy}^{mm}, \quad (11)$$

$$3\langle F_{22}^{(2)} \rangle = Q_{xx}^{ll} + Q_{yy}^{mm} - Q_{yy}^{ll} - Q_{xx}^{mm}. \quad (12)$$

Note that the same order parameters must have the same values in all the ways they are computed. The values of the order parameters depend on the phase orientation. For the completely ordered system, there are six main phase orientations which are summarized in Table I. The $\langle F_{00}^{(2)} \rangle$ order parameter is a measure of the alignment of the \mathbf{n} molecule axis along the Z axis of the reference frame. The $\langle F_{02}^{(2)} \rangle$ order parameter describes the relative distribution of the \mathbf{l} and the \mathbf{m} axes along the Z axis. Both $\langle F_{00}^{(2)} \rangle$ and $\langle F_{02}^{(2)} \rangle$ can be nonzero in the uniaxial nematic phase. The $\langle F_{20}^{(2)} \rangle$ order parameter describes the relative distribution of the \mathbf{n} axis along the X and the Y axes. The $\langle F_{22}^{(2)} \rangle$ order parameter is related to the distributions of the \mathbf{l} and \mathbf{m} axes along the X and the Y axes. Both $\langle F_{20}^{(2)} \rangle$ and $\langle F_{22}^{(2)} \rangle$ signal the biaxiality of the phase.

4. Results

Prior to studying the confined systems, we have calculated the homogeneous bulk system and the temperature dependence of the order parameters, as shown in Fig. 1. We have performed MC simulations on $10 \times 10 \times 10$ and $16 \times 16 \times 16$ lattices with periodic boundary conditions in all three directions. The temperature step was typically 0.1 and 0.01 near the $I-N_B$ transition. We have used 10^4 lattice cycles for warm-up and 10^4 cycles for production, where a cycle is N attempted moves. Sometimes 10^5 cycles were used as an additional check. We started from the ideal configuration at the lowest temperature, then the last configuration for a given temperature was used as the initial configuration for the next temperature. Figure 1 shows that the biaxial-isotropic transition is near $T^* = 1.2(1)$, in

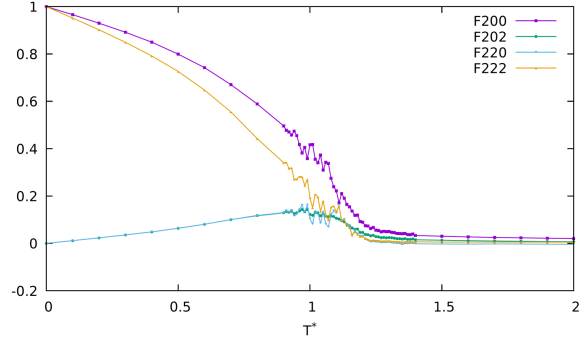


Fig. 1. Order parameters $\langle F_{\mu\nu}^{(j)} \rangle$ ($F_{j\mu\nu}$ in the picture) vs temperature for the homogeneous system. Results obtained from $16 \times 16 \times 16$ MC (no walls) for $\lambda = 1/\sqrt{3}$. The biaxial-isotropic transition is near $T^* = 1.2(1)$. Large fluctuations of the order parameters are present below the transition point.

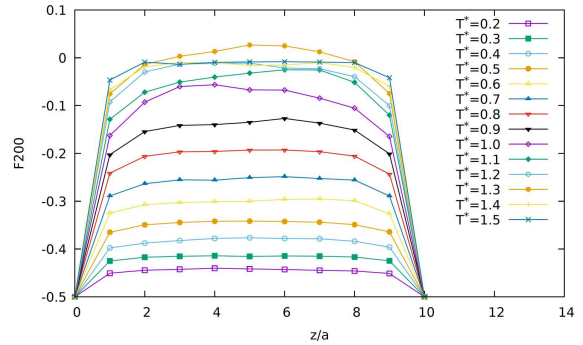


Fig. 2. The profiles of $\langle F_{00}^{(2)} \rangle$ as functions of z for the confined system between two walls. Results obtained from $10 \times 10 \times 11$ MC (two walls) for $\lambda = 1/\sqrt{3}$. The isotropic phase in the bulk is present for $T^* \geq 1.3$.

agreement with [21], and $T^* = k_B T/\epsilon$ is the dimensionless temperature, where k_B is the Boltzmann constant. The energy of the homogeneous system is always negative and it is an increasing function of temperature.

Let us move to the description of the confined systems. We have performed MC simulations on $10 \times 10 \times N_z$ lattices, N_z from 3 to 19, with periodic boundary conditions in the X, Y directions and two

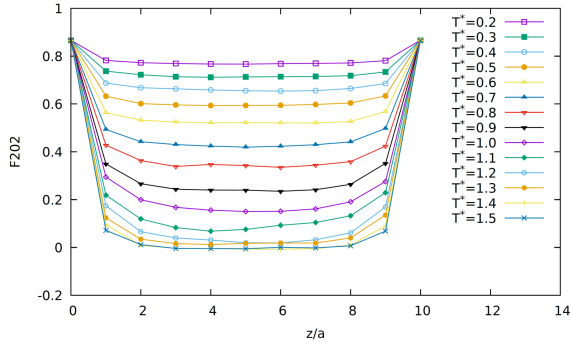


Fig. 3. The profiles of $\langle F_{02}^{(2)} \rangle$ as functions of z for the confined system between two walls. Results obtained from $10 \times 10 \times 11$ MC (two walls) for $\lambda = 1/\sqrt{3}$. The isotropic phase in the bulk is present for $T^* \geq 1.3$.

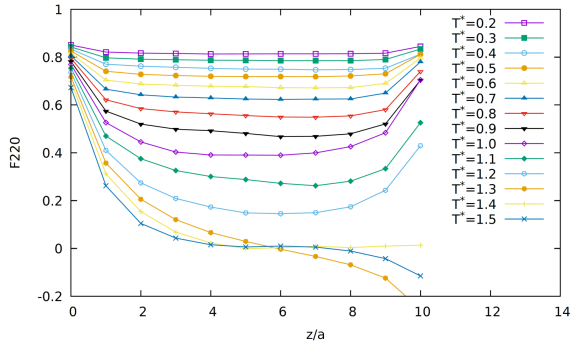


Fig. 4. The profiles of $\langle F_{20}^{(2)} \rangle$ as functions of z for the confined system between two walls. Results obtained from $10 \times 10 \times 11$ MC (two walls) for $\lambda = 1/\sqrt{3}$. The isotropic phase in the bulk is present for $T^* \geq 1.3$. Different preferable orientations on the walls are visible for high temperatures.

parallel walls with planar anchoring. Figures 2–5 show the order parameters $\langle F_{\mu\nu}^{(2)} \rangle$ profiles for the lattice system $10 \times 10 \times 11$. In the isotropic phase ($T^* > 1.3$), the order parameters are almost zero except in the surface layers of the length of approximately 4–5 lattice constants. Near the walls, long molecule axes are nearly parallel to the walls and this yields $\langle F_{00}^{(2)} \rangle < 0$, with the expected limit of $-1/2$ on the walls. On decreasing temperature, a transition takes place to the biaxial nematic phase, at which all order parameters become finite beyond the surface layers. Snapshots of simulation configurations in the biaxial nematic and in the isotropic phases are given in Fig. 6 and 7, respectively. In the biaxial nematic phase, the preferable orientation of molecules on both walls is the same, although it is changing during computations. In the isotropic phase, different preferable orientations on the walls are common which is visible in the snapshots and the order parameter profiles. We note that this effect cannot be obtained using the boundary conditions with mirror symmetry.

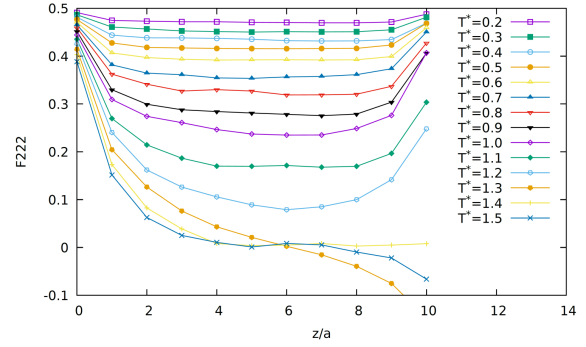


Fig. 5. The profiles of $\langle F_{22}^{(2)} \rangle$ as functions of z for the confined system between two walls. Results obtained from $10 \times 10 \times 11$ MC (two walls) for $\lambda = 1/\sqrt{3}$. The isotropic phase in the bulk is present for $T^* \geq 1.3$. Different preferable orientations on the walls are visible for high temperatures.

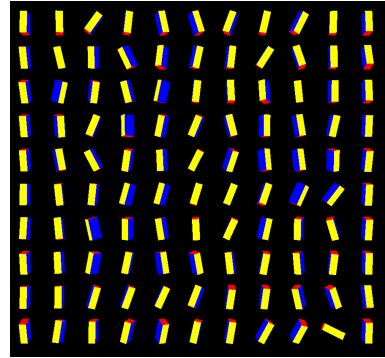


Fig. 6. A snapshot of simulation configuration (YZ layer) in the biaxial nematic phase at $T^* = 0.5$ for the confined system between two walls. Results obtained from $10 \times 10 \times 11$ MC (two walls) for $\lambda = 1/\sqrt{3}$. Long molecule axes are parallel to the Y axis, short molecule axes are parallel to the Z axis.

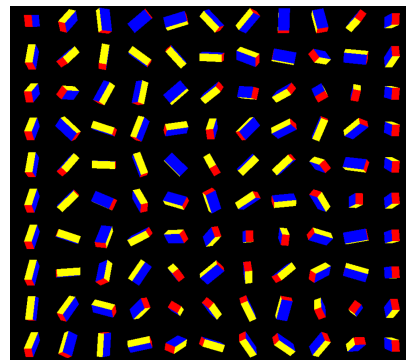


Fig. 7. A snapshot of simulation configuration (YZ layer) in the isotropic phase at $T^* = 1.5$ for the confined system between two walls. Results obtained from $10 \times 10 \times 11$ MC (two walls) for $\lambda = 1/\sqrt{3}$. The preferred orientations of the molecules on both walls (the left and the right columns) are different.

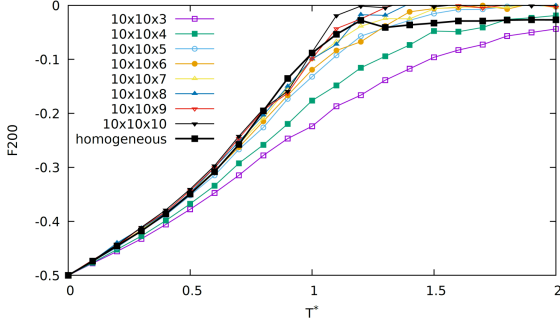


Fig. 8. Temperature dependence of the order parameter $\langle F_{00}^{(2)} \rangle$ for the confined systems between two walls in the cell center. The homogeneous system has a $10 \times 10 \times 10$ lattice.

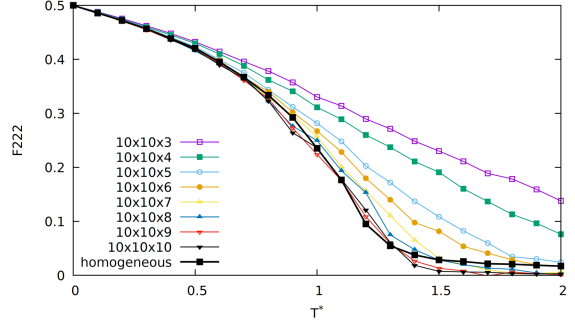


Fig. 11. Temperature dependence of the order parameter $\langle F_{22}^{(2)} \rangle$ for the confined systems between two walls in the cell center. The homogeneous system has a $10 \times 10 \times 10$ lattice.

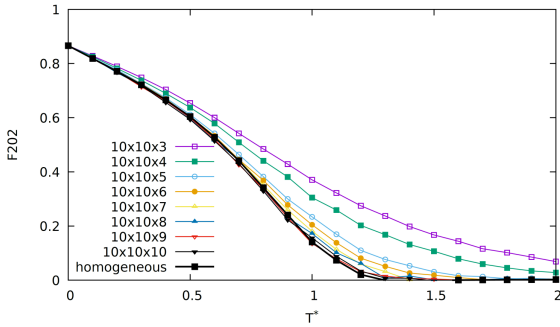


Fig. 9. Temperature dependence of the order parameter $\langle F_{02}^{(2)} \rangle$ for the confined systems between two walls in the cell center. The homogeneous system has a $10 \times 10 \times 10$ lattice.

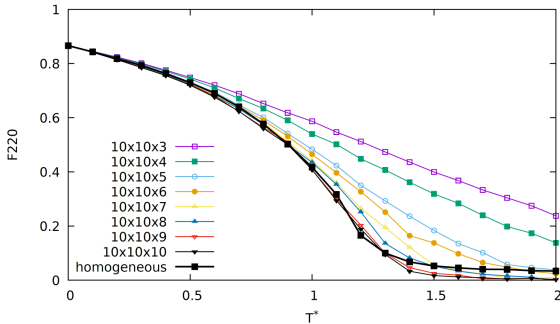


Fig. 10. Temperature dependence of the order parameter $\langle F_{20}^{(2)} \rangle$ for the confined systems between two walls in the cell center. The homogeneous system has a $10 \times 10 \times 10$ lattice.

Figures 8–11 show the temperature dependence of the order parameters in the cell center. The temperature of the isotropic–biaxial transition is shifted but for $N_z > 10$ it is almost the same as in the homogeneous system. From this point the surface layers are separated and they have both biaxial nematic ordering ($\langle F_{22}^{(2)} \rangle$ is nonzero). We note a small discrepancy between the results for the

homogeneous system and for the confined systems. This is due to finite size effects which are more pronounced for the homogeneous system. We note that the difference between the values of the order parameters calculated using different methods in (9)–(12) is less than 10^{-6} . For $N_z = 3$ and $N_z = 4$, the biaxial nematic phase is present in the cell for higher temperatures but the order parameters monotonically go to zero. We have not found any capillary nematization transition.

5. Conclusions

In this work we have studied the order-parameter profiles in the confined systems of optimal biaxial molecules using Monte Carlo simulations in an extended Lebwohl–Lasher model. In the homogeneous system, there is a direct second-order isotropic–biaxial transition. We have studied the confined systems with two parallel walls with planar anchoring and with different wall separations.

For large wall separations, there are surface layers on both walls with the width of ≈ 4 –5 lattice constants and beyond the surface layers the order parameters have values as in the homogeneous system. The ordering within the surface layers is always biaxial whereas in [34] biaxiality close to the wall was present only if the phase was biaxial in the bulk. The reason for this discrepancy is planar anchoring on the walls which creates the planar (uniaxial) Lebwohl–Lasher model with the Kosterlitz–Thouless transition [37, 38]. In our systems, there are additional (biaxial) interactions with neighbors from the second layer. The partial ordering on the walls in our finite systems creates the biaxial ordering in the surface layers for all temperatures. We note that the surface transition was studied, for uniaxial molecules and different surface couplings, using the Landau–de Gennes approach [39, 40]. Additional effects due to external fields were studied in [41] but again for uniaxial molecules.

For small wall separations, the isotropic–biaxial transition is shifted to higher temperatures and

the surface layers are thinner. The preferable orientation of the biaxial nematic phase is approximately the same near the walls and in the center of the cell but its direction can change during simulations. Above the isotropic–biaxial transition, the preferable orientations in both surface layers can be different.

The presented results of MC simulations revealed effects which combine the properties of two-dimensional and three-dimensional systems. Similar results can be obtained in the case of homogeneous anchoring where the long molecule axes are parallel to the specified direction, the same for both walls. In this case, the isotropic–biaxial transition is shifted to even higher temperatures.

References

- [1] M.J. Freiser, *Phys. Rev. Lett.* **24**, 1041 (1970).
- [2] J.P. Straley, *Phys. Rev. A* **10**, 1881 (1974).
- [3] G. Luckhurst, C. Zannoni, P. Nordio, U. Segre, *Mol. Phys.* **30**, 1345 (1975).
- [4] B. Mulder, T. Ruijgrok, *Physica A* **113**, 145 (1982).
- [5] C. Shih, R. Alben, *J. Chem. Phys.* **57**, 3055 (1972).
- [6] W. Li, K.F. Freed, *J. Chem. Phys.* **101**, 519 (1994).
- [7] B. Mulder, *Phys. Rev. A* **39**, 360 (1989).
- [8] M.P. Allen, *Liq. Cryst.* **8**, 499 (1990).
- [9] P.J. Camp, M.P. Allen, *J. Chem. Phys.* **106**, 6681 (1997).
- [10] R.A. Skutnik, I.S. Geier, M. Schoen, *Mol. Phys.* **118**, e1726520 (2020).
- [11] J.H. Lee, T.-K. Lim, W.-T. Kim, J.-I. Jin, *J. Appl. Phys.* **101**, 034105 (2007).
- [12] R. Berardi, L. Muccioli, C. Zannoni, *J. Chem. Phys.* **128**, 024905 (2008).
- [13] B.M. Mulder, *Liq. Cryst.* **1**, 539 (1986).
- [14] D. Allender, L. Longa, *Phys. Rev. E* **78**, 011704 (2008).
- [15] P.K. Mukherjee, K. Sen, *J. Chem. Phys.* **130**, 141101 (2009).
- [16] P.A. Lebwohl, G. Lasher, *Phys. Rev. A* **6**, 426 (1972).
- [17] U. Fabbri, C. Zannoni, *Mol. Phys.* **58**, 763 (1986).
- [18] Z. Zhang, O.G. Mouritsen, M.J. Zuckermann, *Phys. Rev. Lett.* **69**, 2803 (1992).
- [19] C.W. Greeff, M.A. Lee, *Phys. Rev. E* **49**, 3225 (1994).
- [20] S. Boschi, M.P. Brunelli, C. Zannoni, C. Chiccoli, P. Pasini, *Int. J. Mod. Phys. C* **08**, 547 (1997).
- [21] F. Biscarini, C. Chiccoli, P. Pasini, F. Semeria, C. Zannoni, *Phys. Rev. Lett.* **75**, 1803 (1995).
- [22] P. Sheng, *Phys. Rev. Lett.* **37**, 1059 (1976).
- [23] P. Sheng, *Phys. Rev. A* **26**, 1610 (1982).
- [24] Y. Mao, P. Bladon, H.N.W. Lekkerkerker, M.E. Cates, *Mol. Phys.* **92**, 151 (1997).
- [25] Y. Mao, M.E. Cates, H.N.W. Lekkerkerker, *J. Chem. Phys.* **106**, 3721 (1997).
- [26] R. van Roij, M. Dijkstra, R. Evans, *Europhys. Lett.* **49**, 350 (2000).
- [27] R. van Roij, M. Dijkstra, R. Evans, *J. Chem. Phys.* **113**, 7689 (2000).
- [28] M. Dijkstra, R. Roij, R. Evans, *Phys. Rev. E* **63**, 051703 (2001).
- [29] M.P. Allen, *J. Chem. Phys.* **112**, 5447 (2000).
- [30] A. Chrzanowska, P.I.C. Teixeira, H. Ehrentraut, D.J. Cleaver, *J. Phys. Condens. Matter.* **13**, 4715 (2001).
- [31] F. Batalioto, L. Evangelista, G. Barbero, *Phys. Lett. A* **324**, 198 (2004).
- [32] M.J. Green, R.A. Brown, R.C. Armstrong, *J. Comput. Theor. Nanosci.* **7**, 693 (2010).
- [33] R. Aliabadi, M. Moradi, S. Varga, *Phys. Rev. E* **92**, 032503 (2015).
- [34] A. Kapanowski, M. Abram, *Phys. Rev. E* **89**, 062503 (2014).
- [35] F.J. Vesely, *J. Comput. Phys.* **47**, 291 (1982).
- [36] A. Kapanowski, *Phys. Rev. E* **55**, 7090 (1997).
- [37] C. Chiccoli, P. Pasini, C. Zannoni, *Physica A* **148**, 298 (1988).
- [38] E. Mondal, S.K. Roy, *Phys. Lett. A* **312**, 397 (2003).
- [39] Y. L'vov, R.M. Hornreich, D.W. Allender, *Phys. Rev. E* **48**, 1115 (1993).
- [40] N. Kothekar, D.W. Allender, R.M. Hornreich, *Phys. Rev. E* **49**, 2150 (1994).
- [41] M. Ito, M. Torikai, M. Yamashita, *Mol. Cryst. Liq. Cryst.* **441**, 69 (2005).